J. Fluid Mech. (1991), *vol.* 227, *pp.* 273–292
Printed in Great Britain

Liquid-metal flow in a backward elbow in the plane of a strong magnetic field

By T. J. MOON[1], T. Q. HUA[2] AND J. S. WALKER[3]

[1] Mechanical Engineering Department, The University of Texas at Austin, Austin, TX 78712-1063, USA

[2] Engineering Physics Division, Argonne National Laboratory, Argonne, IL 60439, USA

[3] Department of Mechanical and Industrial Engineering, University of Illinois, Urbana, IL 61801, USA

(Received 27 February 1990)

This paper treats a liquid-metal flow through a sharp elbow connecting two constant-area, rectangular ducts with thin metal walls. There is a uniform, strong magnetic field in the plane of the ducts' centrelines, and the velocity component normal to the magnetic field is in opposite directions upstream and downstream of the elbow. The magnetic field is sufficiently strong that inertial effects are negligible everywhere and viscous effects are confined to boundary layers and to an interior layer lying along the magnetic field lines through the inside corner of the elbow. The interior layer involves large velocities parallel to the magnetic field and carries roughly half of the flow between the upstream and downstream ducts for the case considered.

1. Introduction

An elbow in the plane of a locally uniform magnetic field arises in several technologically important liquid-metal magnetohydrodynamic (MHD) flows. For example, several recent designs for liquid-lithium cooling systems for magnetic-confinement fusion reactors involve an elbow between a duct which is nearly perpendicular to the local magnetic field and a duct which is nearly parallel to the field (Smith *et al.* 1985; Malang *et al.* 1988). For fully developed flow in an infinitely long, constant-area duct with a skewed, uniform magnetic field, the pressure gradient is proportional to $\sigma U_0 B_0^2 \sin^2\alpha$, where σ is the electrical conductivity of the liquid metal, U_0 is the average velocity parallel to the duct's centreline, B_0 is the strength of the magnetic field and α is the angle between the magnetic field and the duct's centreline. In the fusion-reaction designs, the ducts near the plasma are nearly parallel to the local magnetic field, so that the high velocity needed for adequate heat removal can be achieved with acceptable pressure drop because $\sin\alpha$ is relatively small. The feeder ducts further from the plasma must be nearly perpendicular to the magnetic field, but U_0 can be much smaller here because these ducts receive very little energy from the plasma.

The fusion-reactor design studies indicate the importance of three unanswered questions about the three-dimensional flow in the elbow between a nearly parallel and a nearly perpendicular duct. Is the elbow pressure drop so large that it negates the benefit of making the energy-collecting ducts nearly parallel to the local field? Does the three-dimensional flow in the elbow involve a large or small velocity along the elbow wall near the plasma? Does the flow in the nearly parallel duct deviate from fully developed for a long distance from the elbow? While the present study is

motivated by the need for reliable fusion-reactor design predictions, our objective is a basic understanding of liquid-metal flows in sharp elbows in the plane of strong, uniform magnetic field.

Four important dimensionless parameters are the magnetic Reynolds number R_m, the interaction parameter N, the Hartmann number M and the wall conductance ratio c, defined by

$$R_m = \mu_p \sigma U_0 L, \quad N = \frac{\sigma B_0^2 L}{\rho U_0}, \quad M = B_0 L\left(\frac{\sigma}{\mu}\right)^{\frac{1}{2}}, \quad c = \frac{\sigma_w t}{\sigma L}.$$

Here, μ_p, ρ and μ are the magnetic permeability, density and viscosity of the liquid metal; L is the characteristic dimension of the duct's cross-section; σ_w and t are the electrical conductivity and thickness of the duct's walls. There is an 'applied' magnetic field, which is produced by the superconducting coils and the plasma current in a magnetic-confinement fusion reactor, and there is an 'induced' magnetic field due to the electric currents in the liquid metal and duct walls. The characteristic ratio of the induced to applied magnetic field is R_m, with typical values of 0.01 to 0.1 for fusion reactors. We assume that R_m is sufficiently small that the induced magnetic field is negligible, while the uniform, applied magnetic field is $\boldsymbol{B} = B_0 \hat{\boldsymbol{y}}$, where $\hat{\boldsymbol{x}}$, $\hat{\boldsymbol{y}}$ and $\hat{\boldsymbol{z}}$ are unit vectors for the Cartesian coordinates with the y-axis parallel to the magnetic field.

In the Navier–Stokes equations, the characteristic ratios of the electromagnetic body force term, $\boldsymbol{j}^* \times \boldsymbol{B}$, to the inertial and viscous terms are N and M^2, respectively, where $\boldsymbol{j}^*$ and $\boldsymbol{j}$ denote the dimensional and dimensionless electric current densities, respectively. Typical values of N and M for liquid-lithium fusion cooling systems range from 10^4 to 10^5. We assume that N is sufficiently large that inertial effects are negligible everywhere and that M is sufficiently large that viscous effects are confined to thin boundary layers and to interior layers which are parallel to the magnetic field. The present solution involves large, $O(M^{\frac{1}{2}})$ dimensionless velocities inside boundary and interior layers with $O(M^{-\frac{1}{2}})$ dimensionless thicknesses. All lengths are normalized by L. Inertial effects in such high-velocity layers are only negligible if $N \gg M^{\frac{3}{2}}$ (Walker, Ludford & Hunt 1971). While this condition is not generally satisfied in fusion-reactor cooling systems, the inertialess predictions agree well with experimental measurements in rectangular ducts for $N = 126000$ and $M = 5800$, and also for $N = 540$ and $M = 2900$ (Hua *et al.* 1988).

The parameter of primary interest here is c. If $c \ll M^{-1}$ or $c \gg M^{\frac{1}{2}}$, then the walls can be treated as electrical insulators or perfect conductors, respectively (Walker 1981). While there is an effort to develop ceramic insulators which are compatible with hot liquid lithium, such insulators do not exist at present, so that most fusion design studies assume that metal walls will be necessary. A typical value of c for liquid lithium in contact with the structural stainless steel walls is 0.1, while a typical value for a steel liner which is electrically insulated from the structural walls is 0.01. If c and (t/L) are both treated as arbitrary, $O(1)$ parameters, then the electrical variables in each wall are coupled to the liquid-metal variables, leading to rather complex problems. For $t \ll L$, the electric potential in each wall is independent of the coordinate normal to the surface of the wall, neglecting $O(t^2/L^2)$ terms (Shercliff 1956). If we assume that there is an electrical insulator at the outside surface of each wall, Shercliff's thin-wall approximation leads to a boundary condition on the liquid-metal variables evaluated at the wall (Holroyd & Walker 1978). If the wall separates two liquid-metal regions, then Shercliff's thin-wall approximation leads to a

condition on the jump in normal electric current density through the wall (Hua & Picologlou 1990). The parameter c appears in these boundary or jump conditions.

Since the σ_w of stainless steel is roughly one-third of the σ for liquid lithium, Shercliff's thin-wall assumption that $t \ll L$ appears to imply the assumption $c \ll 1$. For a long time, the small-c assumption,

$$M^{-1} \ll c \ll 1,$$

was thought to be appropriate for liquid-lithium fusion-reactor flows (Walker & Ludford 1975; Hunt & Holroyd 1977). This assumption states that the bulk or core of the liquid metal has a much lower electrical resistance than the duct wall, which in turn has a much lower electrical resistance than the Hartmann layer with $O(M^{-1})$ thickness adjacent to the wall. When the thin-wall boundary condition with $c \ll 1$ is applied to the inviscid, inertialess core solutions first presented by Kulikovskii (1968), certain characteristic surfaces become important. For a uniform magnetic field, each characteristic surface is composed of the magnetic field lines with the same distance between their intersections with the duct walls. For $O(1)$ distances, the $O(1)$ velocity and the $O(c^{\frac{1}{2}})$ electric current density must follow these characteristic surfaces; only over large, $O(c^{-\frac{1}{2}})$ distances can the flow and electric current leak across these surfaces (Walker & Ludford 1975; Holroyd & Walker 1978).

Recent experiments at Argonne National Laboratory indicate that the predictions of the small-c asymptotic solutions with their characteristic surfaces do not agree with experimental measurements for large values of N and M and for $c = 0.01$ to 0.1 (Picologlou *et al.* 1986). The ratio of the component of velocity or electric current density, which is perpendicular to a characteristic surface, to the corresponding component, which is parallel to the surface, is given by a factor times $c^{\frac{1}{2}}$. This factor depends on the geometry and magnetic-field variation. For circular ducts, this factor is well characterized by λ_1, the first eigenvalue for the problem of decay to fully developed flow, where λ_1 is approximately 10. Therefore, the flow and electric current are only constrained to follow the characteristic surfaces if $\lambda_1 c^{\frac{1}{2}} \ll 1$, which is not true for $c = 0.01$ to 0.1. The experiments show that the characteristic surfaces represent trends rather than rigid guides. The characteristic-surface solutions predict large central regions of virtually stagnant fluid with high-velocity jets adjacent to certain walls, while the observed flows for $c = 0.01$ to 0.1 involve larger velocities near the walls than in the central regions, but no stagnant regions.

Talmage & Walker (1988) use Shercliff's thin-wall approximation, which neglects $O(t^2/L^2)$ terms and which decouples the liquid-metal variables from the wall variables, but they keep c as an $O(1)$, specifiable parameter. The core solutions do not involve characteristic surfaces. Instead, the velocity and electric current in each core are governed by coupled, two-dimensional, elliptic equations in x and z. The predictions of the arbitrary-c solutions agree well with experimental measurements for $c = 0.01$ to 0.1 (Talmage & Walker 1988; Hua *et al.* 1988). Here we treat the flow in a sharp elbow with the assumptions that $R_m \ll 1, N \gg M^{\frac{3}{2}}, M \gg 1, t \ll L$, and $c = O(1)$, and we compare the results to the solutions for the small-c assumption.

Longitudinal sections of a forward elbow and a backward elbow are presented in figure 1. The Cartesian coordinates are oriented with the y-axis parallel to the magnetic field, so that p and $\boldsymbol{j}$ are independent of y, while ϕ and $\boldsymbol{v}$ are linear in y, in the inertialess, inviscid core solutions (Kulikovskii 1968). Here, p and ϕ are the dimensionless pressure and electric potential function, while $\boldsymbol{v} = u\hat{\boldsymbol{x}} + v\hat{\boldsymbol{y}} + w\hat{\boldsymbol{z}}$ is the dimensionless fluid velocity. Each elbow has parallel sides, which are perpendicular to the z-axis, and L is chosen as half the distance between the sides. In dimensionless

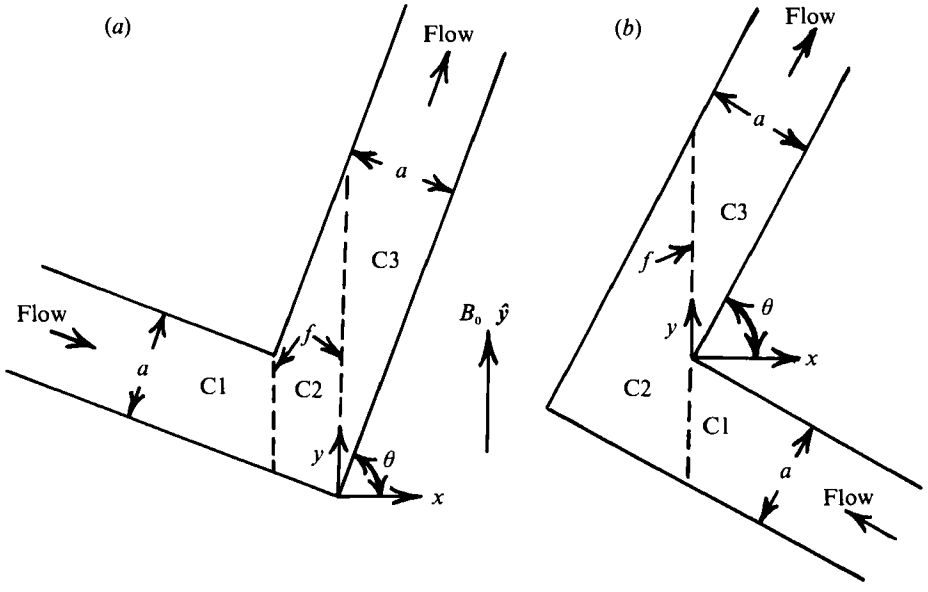

FIGURE 1. Longitudinal sections of two sharp elbows. The parallel sides are at $z = \pm 1$, where the coordinates are normalized by L which is half the distance between the sides. The three inviscid core regions, C1, C2, and C3 are separated by interior or free shear layers f. (*a*) Forward elbow in which the x-component of velocity u is positive everywhere. (*b*) Backward elbow in which u is positive and negative in the downstream and upstream ducts, respectively.

coordinates, the sides are at $z = \pm 1$, while the dimensionless distance a between the top and bottom is the same for the upstream and downstream rectangular ducts. For the arbitrary-c solution, there are three successive core regions, C1, C2 and C3, which are separated by one or two interior layers f with $O(M^{-\frac{1}{2}})$ thickness at $x = 0$ and at $x = x_0 = a(\cos\theta - \sin\theta)$, in the forward elbow. For the upstream or downstream duct in either elbow, the angle between the magnetic field and the duct's centreline is $\alpha = \theta$ or $\alpha = 90° - \theta$, respectively. Each core region is separated from the top or bottom by a Hartmann layer with $O(M^{-1})$ thickness and from each side by a side layer with $O(M^{-\frac{1}{2}})$ thickness. The side layers involve $O(M^{\frac{1}{2}})$ dimensionless values of u and v, so that they carry part of the $O(1)$ total volume flux, even for fully developed flow. Since the distance a between the top and bottom is the same upstream and downstream, U_0 is the total volumetric flow rate, divided by $2aL^2$. For the small-c solutions there is an additional outer side layer with $O(c^{\frac{1}{2}})$ thickness between the inner, viscous side layer with $O(M^{-\frac{1}{2}})$ thickness and the core C2 for either elbow. The outer side layer is inviscid and arises from the Shercliff thin-wall approximation at the top and bottom for $c \ll 1$ and for non-parallel top and bottom (Walker 1981).

All electric currents are driven by the dimensionless induced electric field,

$$\boldsymbol{v} \times \hat{\boldsymbol{y}} = -w\hat{\boldsymbol{x}} + u\hat{\boldsymbol{z}}.$$

For fully devcloped flow in a skewed field, u is proportional to $\sin\alpha$, since $\boldsymbol{v}$ is parallel to the duct's centreline, and the induced electric field drives an electric current circulation through the liquid metal and walls in each cross-section. When two ducts are joined through an elbow, expansion, or manifold, the upstream and downstream fully developed induced electric fields are generally different, and the difference drives an additional three-dimensional electric current circulation near the junction.

For example, if the upstream and downstream induced electric fields have the same sign, but the upstream one is larger, then the three-dimensional electric current circulation increases and decreases the magnitudes of j_z upstream and downstream, respectively. It often reverses the sign of j_z downstream. Since the fully developed electric current must flow through the walls, its magnitude is controlled by the resistance of these walls and is proportional to c. The three-dimensional electric current involves currents between the upstream and downstream ducts through both the walls and the liquid metal. At least part of the three-dimensional current circulates entirely in the liquid metal, so that its magnitude may be much larger than the fully developed current. For the small-c solutions, the three-dimensional current is generally $O(c^{\frac{1}{2}})$ because of its restriction to the characteristic surfaces. The local pressure gradient is proportional to j_z. For our example, the upstream j_z and associated pressure gradient are much larger than those for fully developed flow. If the downstream j_z is reversed by the three-dimensional current, then there is a small pressure recovery. The difference between the large, extra upstream pressure drop and the small downstream pressure recovery is the three-dimensional pressure drop Δp_{3D} which is added to the pressure drops for undisturbed fully developed flow in the upstream and downstream ducts.

The forward elbow with $\theta = 45°$ involves virtually no three-dimensional effects, because the upstream and downstream fully developed induced electric fields are identical. There is no C2 core, the two interior layers merge into one layer through both corners, and the flow is fully developed throughout C1 and C3. The role of the interior layer f is to match the jump from $v < 0$ upstream to $v > 0$ downstream. As θ for a forward elbow increases from 45°, the upstream and downstream induced electric fields increase and decrease, respectively, so that the three-dimensional electric current circulation and other three-dimensional effects increase. Since the flow is inertialess, the solutions apply equally well for a reversed flow direction. The flow in either elbow for $\theta < 45°$ is identical to the reverse flow in the corresponding elbow for $\theta > 45°$, so that we need only consider elbows for $45° \leqslant \theta \leqslant 90°$. As $\theta \to 90°$ for a forward elbow, the upstream induced electric field approaches a maximum and the downstream one approaches zero. As θ for a forward elbow increases beyond 90°, this elbow becomes the backward elbow for $\theta < 90°$. As θ decreases from 90° for the backward elbow, the upstream induced electric field decreases, but the downstream one now has the opposite sign and increases in magnitude. The difference between the upstream and downstream induced electric fields and the associated three-dimensional electric current circulation increases as θ decreases from 90° for a backward elbow. The difference reaches a maximum for $\theta = 45°$, i.e. roughly $\sqrt{2}$ for $\theta = 45°$ versus 1 for $\theta = 90°$. Moon & Walker (1990) present arbitrary-c solutions for the forward elbow for $\tan\theta = 10$. Here we present the arbitrary-c solution for the backward elbow for $\theta = 45°$. Neither analysis applies for $\theta = 90°$, but the solutions do yield some qualitative conclusions about this special case, which are discussed in the final section.

The general properties of the small-c solutions for the forward and backward elbows follow from the small-c asymptotic solutions for expansions and contractions (Walker 1981). Neither core C1 nor core C3 has characteristic surfaces because all magnetic fields lines have the same length between the top and bottom in each region. The flows in these cores are governed by elliptic equations in x and z. In C2, the characteristic surfaces are the x = constant sections, so that both the $O(1)$ u and the $O(c^{\frac{1}{2}})$ j_x must be zero in this core. For the forward elbow, all the flow from C1 and C3 is carried by the $O(M^{\frac{1}{2}})$ u and v inside the viscous inner layers at $z = \pm 1$. The

velocities are $O(1)$ inside the outer layers, but make a negligible, $O(c^{\frac{1}{2}})$ contribution to the total dimensionless volume flux $2a$. The three-dimensional electric current between C1 and C3 is $O(c^{\frac{1}{2}})$ and is carried by $O(1)j_x$ and j_y in the outer side layers at $z = \pm 1$. The currents in the walls make a negligible, $O(c)$ contribution. For the backward elbow, there are two flow paths between C1 and C3: the viscous inner layers adjacent to C2 and the interior layer f at $x = 0$. As $|x|$ decreases from ∞, the flows in C1 and C3 for either elbow deviate from fully developed. This deviation involves two changes: (i) part of the core flow is transferred to the side layers, so that the fraction of the total flow in the side layers is larger at $x = 0$ or $x = x_0$ than that for fully developed flow, and (ii) the remaining core flow becomes more concentrated near $z = \pm 1$. The residual core flow at $x = 0$ or $x = x_0$ is carried by the interior layer f to the inner layers adjacent to C2 or, for the backward elbow, from the lower part of f for $y < 0$ to the upper part for $y > 0$.

For the transition from the small-c asymptotic solution to the arbitrary-c solution, the most important changes occur in the core C2 and adjacent side and interior layers. The outer side layers with $O(c^{\frac{1}{2}})$ thickness spread across the entire duct and become the core. The $O(1)$ values of u and v here now carry part of the $O(1)$ volumetric flux, $2a$. For $c \ll 1$, only the viscous side layers carry any $O(1)$ volumetric flux in this region, but for $c = O(1)$, both the viscous side layers and the core C2 carry part of the $O(1)$ flux. In addition, as c increases from small values to arbitrary values, the $O(c)$ three-dimensional electric currents in the walls become comparable to the $O(c^{\frac{1}{2}})$ currents in the outer side layer which has become the core.

For the forward elbow, the interior layers f no longer involve $O(M^{\frac{1}{2}})$ velocities, and the O(1) flow passes unchanged through these layers from C1 to C2 or from C2 to C3. The only role of these interior layers is to match jumps in the $O(1)$ v and w between adjacent cores (Moon & Walker 1990). For the backward elbow, at least one velocity component in the interior layer remains $O(M^{\frac{1}{2}})$, and this layer continues to carry part of the $O(1)$ volumetric flux. We can ignore the details of the interior layer if we apply a solubility condition to the solutions in the adjacent core regions. After stretching the axial coordinate by $M^{\frac{1}{2}}$ for the interior layer, we introduce the expressions for j_x and j_z from the momentum equation into the x- and z-components of Ohm's law. We introduce the resultant expressions for u and w into the conservation of mass equation, $\nabla \cdot \boldsymbol{v} = 0$. We integrate the resultant expression over a $z =$ constant section of the interior layer, i.e. we integrate with respect to y and with respect to the stretched x, and we apply the boundary conditions on v at the walls. The result is the solubility condition that the integral from bottom to top of the core values of j_z must be the same on both sides of the layer (Hua & Picologlou 1990). For the interior layers at $x = x_0$ and at $x = 0$ in the forward elbow, this condition yields the relationships

$$j_{zC1} = j_{zC2} \quad \text{at} \quad x = x_0, \qquad j_{zC2} = j_{zC3} \quad \text{at} \quad x = 0,$$

since j_z is independent of y in each core. There is no jump in j_z across either interior layer in a forward elbow. For the backward elbow, the condition yields the relationship

$$\operatorname{cosec}\theta j_{zC1} + \sec\theta j_{zC3} = (\operatorname{cosec}\theta + \sec\theta) j_{zC2} \quad \text{at} \quad x = 0.$$

There is a jump $(j_{zC2} - j_{zC1})$ across f for $y < 0$ and a jump $(j_{zC2} - j_{zC3})$ of the opposite sign across f for $y > 0$. The interior layer which matches a jump in the $O(1)j_z$ involves an $O(M^{\frac{1}{2}})$ v, so that there is an $O(1)$ volumetric flux parallel to the magnetic field inside this layer. The flow entering f from C1 splits: part enters C2 and part flows vertically upward across the $y = 0$ plane inside the interior layer. The height-averaged

continuity of the core j_z across this layer simply states that all the upward flow inside the interior layer at $y = 0$ must enter C3 for $y > 0$. Therefore, part of the flow completely bypasses the triangular protuberance for $x < 0$ in the backward elbow. For a backward elbow for $\theta > 45°$, there may also be a jump in the $O(1)$ ϕ across the interior layer, while ϕ is always continuous across the interior layers in the forward elbow. This jump in ϕ implies $O(M^{\frac{1}{2}})$ values of w inside this layer. Part of the flow entering f from C1 is carried in the z-direction inside this layer to enter the side layers adjacent to C2 for $y < 0$ and a corresponding lateral flow redistribution for $y > 0$. Here we only consider the backward elbow for $\theta = 45°$, so that ϕ is continuous across f and the only $O(1)$ flow inside f is in the y-direction.

2. Problem formulation

The dimensionless equations governing the steady, inductionless, inertialess flow of a liquid metal with a uniform applied magnetic field and with constant properties are

$$0 = -\nabla p + \boldsymbol{j} \times \hat{\boldsymbol{y}} + M^{-2} \nabla^2 \boldsymbol{v}, \quad \nabla \cdot \boldsymbol{v} = 0, \tag{1a, b}$$

$$\boldsymbol{j} = -\nabla \phi + \boldsymbol{v} \times \hat{\boldsymbol{y}}, \quad \nabla \cdot \boldsymbol{j} = 0, \tag{1c, d}$$

where p, $\boldsymbol{j}$, $\boldsymbol{v}$ and ϕ are normalized by $\sigma U_0 B_0^2 L$, $\sigma U_0 B_0$, U_0 and $U_0 B_0 L$, respectively. Here we treat the backward elbow shown in figure 1 (*b*) with $\theta = 45°$. The inside walls are at $y = \pm x$, for $0 < x < \infty$ and the outside walls are at $y = \pm(x + A)$, for $-A < x < \infty$, where $A = \sqrt{2}a$. The flow is antisymmetric in y and symmetric in z, so that we need only treat the flow for $0 \leqslant y < \infty$ and $-1 \leqslant z \leqslant 0$, with appropriate symmetry conditions at $y = 0$ and at $z = 0$. The boundary conditions at each wall are

$$\boldsymbol{v} = 0, \quad \boldsymbol{j} \cdot \hat{\boldsymbol{n}} = c \nabla_{\mathrm{w}}^2 \phi, \tag{2a, b}$$

where $\hat{\boldsymbol{n}}$ is a unit normal to the wall, into the fluid, and ∇_{w}^2 represents a two-dimensional Laplacian in the plane of the wall (Holroyd & Walker 1978). Here all walls have the same wall conductance ratio c.

For $M \gg 1$, there are inviscid core regions where the last term in the momentum equation (1*a*) is negligible, there are Hartmann layers with $O(M^{-1})$ thickness adjacent to the walls at $y = x$ and at $y = x + A$, there are side layers with $O(M^{-\frac{1}{2}})$ thickness adjacent to the side at $z = -1$, and there is an interior layer with $O(M^{-\frac{1}{2}})$ thickness at $x = 0$. The Hartmann layers satisfy the boundary conditions (2*a*), provided the adjacent core solution satisfies the Hartmann condition

$$v = u \quad \text{at} \quad y = x \quad \text{and at} \quad y = x + A. \tag{3}$$

The jumps in $\boldsymbol{j} \cdot \boldsymbol{n}$ and ϕ across a Hartmann layer are $O(M^{-1})$ and $O(M^{-2})$, respectively, so that the condition (2*b*) can be applied directly to the core solution at $y = x$ and at $y = x + A$ (Walker *et al.* 1971). The side layers involve $O(M^{\frac{1}{2}})$ values of u and v, so that there is a significant fraction of the total flow inside each side layer. However, we can ignore the details of the side layer, provided $c \gg M^{-\frac{1}{2}}$, which is implicit in our assumptions that $c = O(1)$ while $M \gg 1$ (Moon & Walker 1990). Since the jump in j_z across the side layer is $O(M^{-\frac{1}{2}})$, we can apply the boundary condition (2*b*) with the core j_z at $z = -1$ to obtain an equation governing the electric potential function of the sidewall, $\phi_{\mathrm{s}}(x, y)$. The local flow inside the side layer at each value of x and y is proportional to the local jump in the electric potential across the side layer.

3. Numerical solution for core C2

The solution in the core C2 which satisfies (*a*) the inviscid version of the equations (1), (*b*) the symmetry conditions $p = \phi = 0$ at $y = 0$, and (*c*) the Hartmann condition (3) at $y = x+A$ is

$$p = j_x = j_z = 0, \quad j_y = -\frac{\phi_t}{x+A}, \quad \phi = \frac{y\phi_t}{x+A}, \tag{4a–e}$$

$$u = \frac{y}{x+A}\frac{\partial \phi_t}{\partial z}, \quad v = \frac{\partial \phi_t}{\partial z}, \quad w = -y\frac{\partial}{\partial x}\left(\frac{\phi_t}{x+A}\right), \tag{4f–h}$$

where $\phi_t(x, z)$ is the electric potential of the top wall. The boundary condition (2*b*) at $y = x+A$ gives the equation

$$\sqrt{2}c\left(\frac{1}{2}\frac{\partial^2 \phi_t}{\partial x^2}+\frac{\partial^2 \phi_t}{\partial z^2}\right) = \frac{\phi_t}{x+A}, \tag{5}$$

governing $\phi_t(x, z)$ for $-A \leqslant x \leqslant 0$ and $-1 \leqslant z \leqslant 0$. Symmetry provides two boundary conditions for (5), namely

$$\phi_t(-A, z) = 0, \quad \phi_t(x, 0) = 0. \tag{6a,b}$$

The boundary condition (2*b*) at $z = -1$ gives the Laplace equation

$$\frac{\partial^2 \phi_s}{\partial x^2}+\frac{\partial^2 \phi_s}{\partial y^2} = 0 \tag{7}$$

governing the electric potential of the side wall $\phi_s(x, y)$ for the triangular area $-A \leqslant x \leqslant 0$, $0 \leqslant y \leqslant x+A$. Symmetry gives the boundary condition

$$\phi_s(x, 0) = 0. \tag{8}$$

At the intersection of the top and side at $y = x+A$ and $z = -1$, the electric potentials in the two walls must be equal. In addition, the electric current leaving the side at $y = x+A$ must equal the current entering the top at $z = -1$ because the currents diverted within the walls and entering the side layer are $O(t/L)$ and $O(M^{-\frac{1}{2}})$, respectively. Therefore, the top potential ϕ_t and side potential ϕ_s are coupled by the boundary conditions

$$\phi_s = \phi_t, \quad \frac{\partial \phi_s}{\partial y}-\frac{\partial \phi_s}{\partial x} = \sqrt{2}\frac{\partial \phi_t}{\partial z} \quad \text{at} \quad y = x+A, z = -1. \tag{9a,b}$$

The values of ϕ_t and ϕ_s at $x = 0$ are determined by the matching conditions with the core C3 across the interior layer *f*. One component of our iterative solution is a successive-over-relaxation finite-difference solution of (5), (7) with the boundary conditions (6), (8), (9) and with fixed values of ϕ_t and ϕ_s at $x = 0$. In this finite-difference solution we use $\Delta x = \Delta y = h = \frac{1}{14}A$ and $\Delta z = 0.1$, so that all grid spacings are roughly equal. We also used grid spacings which are half these values, and the results are virtually identical.

4. Analytical solution for the core C3

The solutions for the core C3 and for the sidewall electric potential for $x > 0$ are given by the general eigenfunction expansion presented by Moon & Walker (1990) for $\theta = 45°$. In this solution

$$p = C_0 - \frac{2cKx}{a} + \sum_{n=1}^{\infty} C_n \exp(-\lambda_n x)[A_n \cos(\lambda_n z/\sqrt{2}) + B_n \cosh(\alpha_n z)],$$

$$\phi_t + \phi_b = 2Kz + \sum_{n=1}^{\infty} C_n \exp(-\lambda_n x) \sin(\lambda_n z/\sqrt{2}),$$

$$\phi_t - \phi_b = \sum_{n=1}^{\infty} C_n \exp(-\lambda_n x)\left[a\lambda_n A_n \sin(\lambda_n z/\sqrt{2}) + \frac{2^{\frac{3}{2}} B_n \sinh(\alpha_n z)}{c\alpha_n}\right],$$

$$\phi_s = -K\left\{1 + \frac{c(y-x)}{\sqrt{2}a}\left[1 - \frac{(y-x)}{\sqrt{2}a}\right]\right\} + \sum_{n=1}^{\infty} C_n \exp(-\lambda_n x)$$

$$\times \left\{\frac{1}{\lambda_n c}[A_n \cos(\lambda_n/\sqrt{2}) + B_n \cosh(\alpha_n)] + \exp[-\tfrac{1}{2}\lambda_n(y-x)]\right.$$

$$\left.\times [D_n \cos(\tfrac{1}{2}\lambda_n(y-x)) + E_n \sin(\tfrac{1}{2}\lambda_n(y-x))]\right\},$$

where $p(x, z)$ is the pressure in the core C3 for $x > 0$; $\phi_t(x, z)$ and $\phi_b(x, z)$ are the electric potentials of the top and bottom walls at $y = x + A$ and at $y = x$, respectively; $\phi_s(x, y)$ is the sidewall electric potential in the parallelogram $0 \leqslant x < \infty$ and $x \leqslant y \leqslant x + A$;

$$K = \frac{1}{\sqrt{2}}\left(1 + \frac{2c}{a} + \frac{a}{6}\right)^{-1}; \quad \text{and} \quad \alpha_n = \left(\frac{2}{ac} - \lambda_n^2\right)^{\frac{1}{2}}.$$

In these solutions, the terms before the summations represent fully developed flow in this constant-area duct which is skewed at 45° to the magnetic field, and the terms after the summations represent the decaying three-dimensional disturbance. The eigenvalues are λ_n, the coefficients of the eigenfunctions are C_n, and the constants within each set of eigenfunctions are A_n, B_n, D_n and E_n. These solutions satisfy (*a*) the inviscid version of (1), (*b*) the Hartmann conditions (3) at $y = x$ and at $y = x + A$, (*c*) the electrical conditions (2*b*) at $y = x$ at $y = x + A$ and at $z = -1$, and (*d*) the symmetry conditions at $z = 0$.

There are five additional conditions at each x = constant cross-section: (*a*) the continuity of the electric potential at $y = x$ or at $y = x + A$ and at $z = -1$, (*b*) the continuity of the electric current between the side and the top or bottom at $y = x + A$ or at $y = x$ and at $z = -1$, and (*c*) a conservation of mass condition which must be applied because we do not treat the side layer, which carries a significant fraction of the flow. The last condition guarantees the existence of a side-layer solution which matches our core solution and our sidewall electric potential. The mass conservation condition is not needed for $x < 0$ because the symmetry guarantees equal and opposite flows in the x-direction for $y > 0$ and $y < 0$. The five conditions at each x = constant cross-section for $x > 0$ give explicit expressions for the internal constants A_n, B_n, D_n and E_n and give a transcendental characteristic equation for the eigenvalues λ_n. For given values of a and c, with $\theta = 45°$, there is an infinite number of discrete eigenvalues; some are real and some are complex, where the complex values are complex conjugates. For the present problem, we only keep the eigenvalues with positive real parts, and we number the eigenvalues with increasing real parts corresponding to increasingly rapid spatial decay with increasing x. The first twenty eigenvalues for $a = 1$ and $c = 0.1$ are: 2.075, 4.164 ± 1.287i, 5.530 ± 1.822i, 6.485, 8.435 ± 2.179i, 10.770, 11.522 ± 4.337i, 12.012 ± 2.706i, 12.914, 15.273, 16.274 ± 2.466i, 16.755 ± 8.899i and 19.530. For this case there are six real eigenvalues and seven pairs of complex conjugates for the first twenty eigenvalues. There is a

shift from real to complex eigenvalues as either θ increases or as c decreases (Moon & Walker 1990). The corresponding values of A_n, B_n, D_n and E_n are not presented here. The remaining unknown coefficients C_n are determined by the matching conditions at $x = 0$. Once the solutions for p, ϕ_t, and ϕ_b are known, the other variables in the core C3 are given by the solution of the inviscid equations (1), namely

$$\phi = \phi_b + \frac{y-x}{A}(\phi_t - \phi_b), \quad j_x = \frac{\partial p}{\partial z}, \quad j_y = \frac{1}{A}(\phi_b - \phi_t), \quad j_z = -\frac{\partial p}{\partial x},$$

$$u = v = \frac{\partial \phi_b}{\partial z} - \frac{\partial p}{\partial x} + \frac{y-x}{A}\left(\frac{\partial \phi_t}{\partial z} - \frac{\partial \phi_b}{\partial z}\right), \quad w = -\frac{\partial \phi}{\partial x} - \frac{\partial p}{\partial z}.$$

5. Matching solutions at $x = 0$

The electric potentials of the inner walls at $y = \pm x$ must have the same value at $x = 0$, and this value is zero by symmetry. The pressure must be continuous across the interior layer f because a jump in the $O(1)$ pressure implies an $O(M^{\frac{1}{2}})j_z$ and an $O(M)v$ inside f. The electric potentials of the top and side are continuous at $x = 0$. In addition, the axial currents in the top and side must be continuous at $x = 0$, because any $O(1)$ electric current from the top or side to the interior layer implies at $O(M^{\frac{1}{2}})j_y$ or j_z and an $O(M)w$ or v, respectively. Therefore, the boundary and matching conditions at $x = 0$ are

$$p(0^+, z) = \phi_b(0^+, z) = 0, \quad \phi_t(0^+, z) = \phi_t(0^-, z), \tag{10a–c}$$

$$\phi_s(0^+, y) = \phi_s(0^-, y), \quad \frac{\partial \phi_t}{\partial x}(0^+, z) = \frac{\partial \phi_t}{\partial x}(0^-, z) \tag{10d, e}$$

$$\frac{\partial \phi_s}{\partial x}(0^+, y) = \frac{\partial \phi_s}{\partial x}(0^-, y). \tag{10f}$$

Here, a variable at $x = 0^+$ is determined from one of the eigenfunction expansions evaluated at $x = 0$, while a variable at $x = 0^-$ is approximated from the discrete values in the finite-difference solution for the core C2 and the adjacent side for $x \leqslant 0$. The conditions (10) determine the coefficients C_n in the eigenfunction expansions and the discrete values of ϕ_t and ϕ_s at $x = 0^-$.

Since we only use the first 20 eigenvalues, there are 21 unknowns in the eigenfunction expansions, including the constant pressure C_0. At $x = 0^-$, there are 10 unknown values of ϕ_t at $z = -1 + 0.1j$, for $j = 0$ to 9, and 13 unknown values of ϕ_s at $y = kh$, for $k = 1$–13. We derive 44 simultaneous, linear equations governing these 44 unknowns, and we solve these equations by Gauss elimination. Twenty-one of the simultaneous equations are derived from the conditions (10a–d) with a method of weighted residuals. The residual to be minimized is defined by

$$R = \int_1^0 \{w_p[p(0^+, z)]^2 + w_b[\phi_b(0^+, z)]^2 + w_t[\phi_t(0^+, z) - \phi_t(0^-, z)]^2\}\,\mathrm{d}z + \int_0^A [\phi_s(0^+, y) - \phi_s(0^-, y)]^2\,\mathrm{d}y,$$

where w_p, w_b and w_t are the weighting factors for the conditions on p, ϕ_b, and ϕ_t, while the weighting factor for the condition on ϕ_s is chosen as one. In order to minimize the residual, we set $\partial R/\partial C_n = 0$, for $n = 0$ to 20, which gives 21 equations. The coefficients C_n are multiplied by sums of integrals of products of the

eigenfunctions at $x = 0$. These integrals are evaluated analytically. There are also integrals of the eigenfunctions times $\phi_t(0^-, z)$ or $\phi_s(0^-, y)$. These functions at $x = 0^-$ are assumed to be piecewise constant over intervals centred at the discrete z- or y-values for the finite-difference solution. The eigenfunctions are integrated analytically over these intervals of length 0.1 or h in order to obtain the coefficients of the unknown discrete values of ϕ_t and ϕ_s at $x = 0^-$ in these 21 equations. The inhomogeneous terms in these equations involve integrals of the fully developed flow solution times eigenfunctions, and these integrals are also evaluated analytically.

The equations (5) and (7) guarantee conservation of electric current in the top and side, respectively. Each interior finite difference equation guarantees conservation of current for (*a*) a rectangular segment of the top, or (*b*) a square segment of the side, or (*c*) a cell composed of a rectangular segment of the top at $z = -1$ and a triangular segment of the side at $y = x + A$. Together, these finite-difference equations guarantee conservation of current for $-A \leqslant x \leqslant -0.5h$. Therefore, we integrate (5) and (7) over segments of the top and side for $-0.5h \leqslant x \leqslant 0$ in order to complete the conservation of current. For the top, the integrals along bounding lines at $x = -0.5h$ and at $z = z_j \pm 0.05$ are evaluated from the discrete values of ϕ_t at $x = 0$ and at $x = -h$, while the integral along the line at $x = 0$ is evaluated analytically from the eigenfunction expansion for ϕ_t through the matching condition (10*e*). For the side, the integrals along bounding lines at $x = -0.5h$ and at $y = y_k \pm 0.5h$ are evaluated from the discrete values of ϕ_s at $x = 0$ and at $x = -h$, while the integral along the line at $x = 0$ is evaluated analytically from the eigenfunction expansion for ϕ_s through the matching condition (10*f*). There is again one special cell consisting of a triangle at the peak of the side and a rectangle of the top at $z = -1$. These conservation-of-current equations for segments in $-0.5h \leqslant x \leqslant 0$ give 23 linear, simultaneous equations for the 21 coefficients C_n and the 23 discrete values of ϕ_t and ϕ_s at $x = 0^-$. The inhomogeneous terms in these equations involve the discrete values of ϕ_t and ϕ_s at $x = -h$. In our solution, we alternately (*a*) determine C_n and the discrete values of ϕ_t and ϕ_s at $x = 0^-$ with given values of ϕ_t and ϕ_s at $x = -h$, and (*b*) determine the discrete values of ϕ_t and ϕ_s for $-A \leqslant x \leqslant -h$ with a successive-over-relaxation scheme and with given values of ϕ_t and ϕ_s at $x = 0^-$. This iterative scheme converges in roughly 20 cycles with 50 iterations of the relaxation scheme in each cycle.

6. Interior layer at $x = 0$

The height-averaged value of $j_z = -\partial p/\partial x$ must be continuous across an interior layer. This condition is automatically satisfied in the present problem because $\partial p/\partial x = 0$ in the core C2, while $\partial p/\partial x$ has equal-magnitude positive and negative values in the equal-height cores C1 and C3, respectively. The jump in $\partial p/\partial x$ across the interior layer implies a jump in u and an $O(M^{\frac{1}{2}})$ v inside f. For the present problem, ϕ is continuous across f, so that $w = O(1)$, and there is no redistribution of the flow in the z-direction inside f. Therefore, part of the flow entering f from C1 flows across the $y = 0$ plane inside f and enters C3, all in the same $z =$ constant plane. The solution in each $z =$ constant plane is independent of the solutions at other z-values and is proportional to the local value of $\partial p/\partial x$ in C3 at $x = 0^+$. Without inertial effects, the interior-layer solution is symmetric about the $y = 0$ plane.

For the interior layer, the leading terms in the asymptotic expansions are

$$u = u_f, \quad v = M^{\frac{1}{2}} v_f, \quad w = w_f, \quad j_x = M^{-\frac{1}{2}} j_{xf}, \quad j_z = j_{zf},$$
$$j_y = -A^{-1}\phi_t(0, z), \quad \phi = A^{-1} y \phi_t(0, z), \quad p = M^{-\frac{1}{2}} p_f,$$

where the variables with a subscript f are functions of (ξ, y, z), and $\xi = M^{\frac{1}{2}} x$ is the stretched axial coordinate. The x- and z-components of the momentum equation $(1a)$ give

$$j_{zf} = -\frac{\partial p_f}{\partial \xi}, \quad j_{xf} = \frac{\partial p_f}{\partial z}, \tag{11}$$

so that $(1d)$ is automatically satisfied. For Ohm's law $(1c)$ the x-component gives an expression for w_f which is of no interest here, the y-component is automatically satisfied, and the z-component gives

$$u_f = \frac{y}{A}\frac{\partial \phi_t}{\partial z}(0, z) - \frac{\partial p_f}{\partial \xi}. \tag{12}$$

The y-component of $(1a)$ and $(1b)$ gives

$$\frac{\partial p_f}{\partial y} = \frac{\partial^2 v_f}{\partial \xi^2}, \quad \frac{\partial v_f}{\partial y} = \frac{\partial^2 p_f}{\partial \xi^2}. \tag{13a, b}$$

The equations (11), (12) give j_{xf}, j_{zf}, and u_f once (13) are solved for p_f and v_f. The Hartmann conditions (3) still apply because the interior layer is much thicker than a Hartmann layer, so that

$$v_f = 0 \quad \text{at} \quad y = A \quad \text{for} \quad -\infty < x < \infty, \tag{14a}$$

$$v_f = 0 \quad \text{at} \quad y = 0 \quad \text{for} \quad 0 < x < \infty. \tag{14b}$$

Symmetry gives

$$\frac{\partial v_f}{\partial y} = 0 \quad \text{at} \quad y = 0 \quad \text{for} \quad -\infty < x < 0. \tag{14c}$$

Matching the C2 and C3 core solutions gives

$$v_f \to 0, \quad p_f \to 0 \quad \text{as} \quad \xi \to -\infty, \tag{15a, b}$$

$$v_f \to 0, \quad p_f \to \xi \frac{\partial p}{\partial x}(0^+, z) + p'(0^+, z) \quad \text{as} \quad \xi \to \infty, \tag{15c, d}$$

where $p'(x, z)$ is the $O(M^{-\frac{1}{2}})$ pressure perturbation in the core C3.

We introduce a stream function $\psi(\xi, y, z)$ where

$$p_f = \frac{\partial p}{\partial x}(0^+, z) \int_{-\infty}^{\xi} \frac{\partial \psi}{\partial y}(\xi^*, y, z)\, \mathrm{d}\xi^*, \tag{16a}$$

$$v_f = \frac{\partial p}{\partial x}(0^+, z) \frac{\partial \psi}{\partial \xi}(\xi, y, z), \tag{16b}$$

so that $(13b)$ is automatically satisfied. The equation $(13a)$ becomes

$$\frac{\partial^2 \psi}{\partial y^2} = \frac{\partial^4 \psi}{\partial \xi^4}. \tag{17}$$

The boundary conditions (14), (15) become

$$\psi = A \quad \text{at} \quad y = A \quad \text{for} \quad -\infty < x < \infty, \tag{18a}$$

$$\psi = 0 \quad \text{at} \quad y = 0 \quad \text{for} \quad 0 < x < \infty, \tag{18b}$$

$$\frac{\partial \psi}{\partial y} = 0 \quad \text{at} \quad y = 0 \quad \text{for} \quad -\infty < x < 0, \tag{18c}$$

$$\psi \to A \quad \text{as} \quad \xi \to -\infty, \qquad \psi \to y \quad \text{as} \quad \xi \to \infty. \tag{18d, e}$$

Talmage *et al.* (1989) present a solution for the boundary-value problem (17), (18) which they derive for a quite different MHD interior layer. In order to interpret their

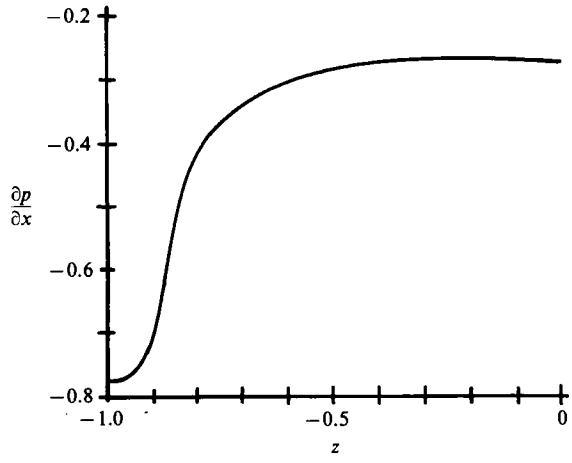

FIGURE 2. Values of $\partial p/\partial x$ in the core C3 at $x = 0^+$.

results for the present interior layer, we rescale the axial coordinate and the vertical velocity with

$$x = M^{-\frac{1}{2}}A^{\frac{1}{2}}X, \quad v = M^{\frac{1}{2}}A^{-\frac{1}{2}}\frac{\partial p}{\partial x}(0^+, z)V.$$

At $y = 0$, there is a discontinuity in V with $V = 0$ for $X > 0$ and $V = 0.7$ at $X = 0^-$. This discontinuity is matched by an $O(M^{-1}) \times O(M^{-1})$ region lying along the edge at $x = y = 0$. As X decreases from 0, V decreases to zero at $X = -2.9$. There is a small negative value of V for $X < -2.9$, which means that as we enter f from C2, v first dips slightly before shooting up to a large value near $x = 0$. As y increases, the peak value of V decreases for two reasons. First, the flow is turning to enter the core C3, so that the vertically upward flow inside f decreases linearly with y. Second the profile of V spreads to positive values of X. At $y = 0.4A$, V is positive for $-2.9 < X < 1.6$, and has a maximum value of 0.278 at $X = -0.5$. At $y = 0.8A$, V is positive for roughly the same range of X, but the peak value is only 0.084 at $X = -0.56$. Finally, the fraction of the total flow crossing the $y = 0$ plane inside the interior layer and thus bypassing the core C2 is given by

$$-\sqrt{2}\int_{-1}^{0}\frac{\partial p}{\partial x}(0^+, z)\,\mathrm{d}z.$$

This expression is obtained by integrating (13*b*) with respect to ξ, y and z, and by using the conditions (14), (15).

7. Results

For the results presented here, $a = 1$ and $c = 0.1$. For the weighted residual R, we choose $w_b = w_t = 1$, so that the three electric potential conditions (10*b–d*) are weighted equally. As c decreases, the magnitudes of the electric potentials increase slightly, as reflected in the value of K, but the magnitude of p decreases roughly proportionally to c. Without a weighting factor, a large relative error in $[p(0^+, z)]^2$ would still make only a minor contribution to R for $c = 0.1$. To compensate for the relative sizes of p and ϕ, we choose $w_p = c^{-2} = 100$.

The graph of $\partial p/\partial x$ in the core C3 at $x = 0^+$ is presented in figure 2. Integrating this graph gives a value of 0.5044 for the fraction of the total flow crossing the $y = 0$ plane

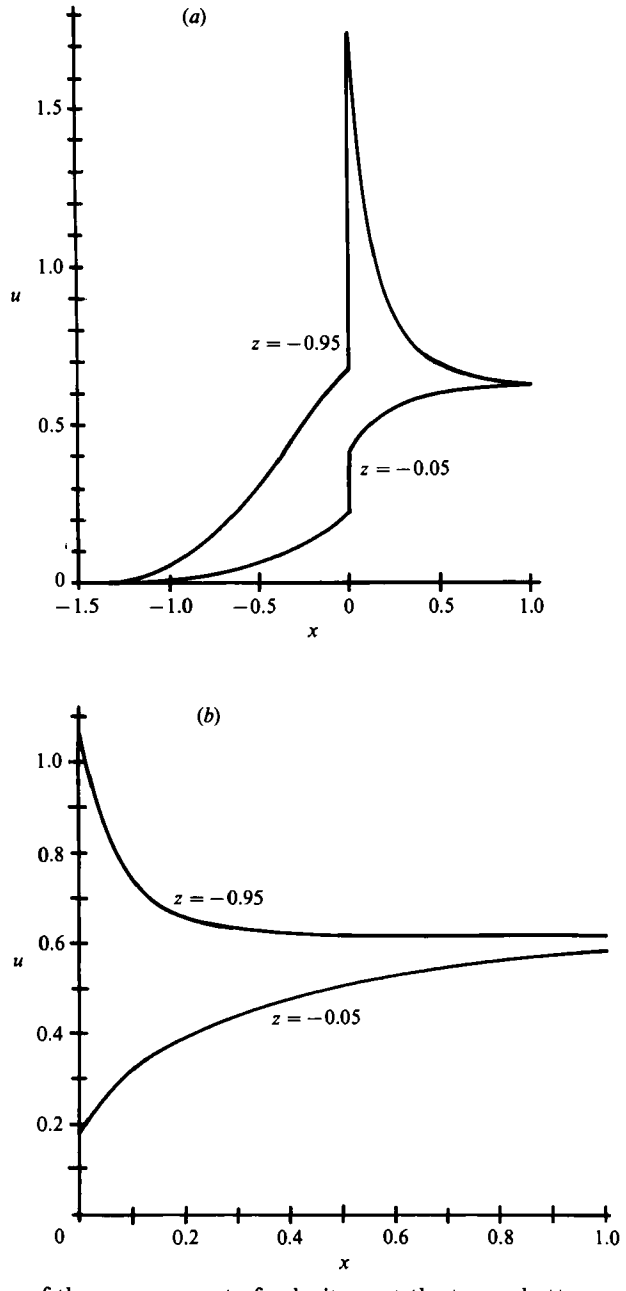

FIGURE 3. Values of the x-component of velocity u at the top or bottom wall and at $z = -0.05$ or at $z = -0.95$. (*a*) u at the top wall at $y = x+A$, for $x > -A$. (*b*) u at the bottom wall at $y = x$, for $x > 0$.

inside the interior layer f, so that roughly half the total flow bypasses the core C2 and adjacent side layers. Since the vertical flow inside f at each z is proportional to the local jump in $\partial p/\partial x$, this flow near $z = -1$ is roughly three times that near $z = 0$. Indeed, half of this vertical flow for $z < 0$ is concentrated in $-1 \leqslant z \leqslant -0.65$.

The plots of u versus x at two values of z and at the top or bottom are presented

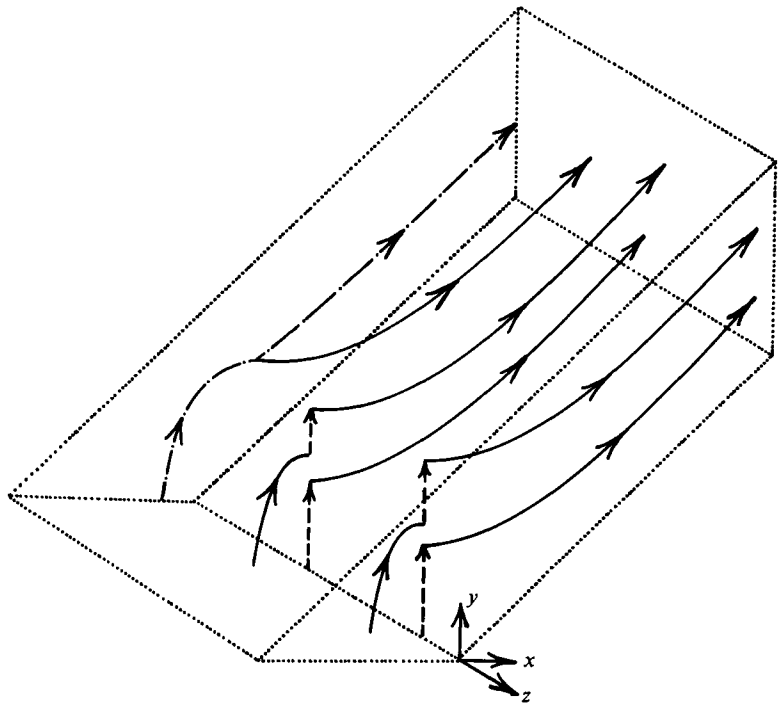

FIGURE 4. Sketch of flow paths from the plane of symmetry $y = 0$ for $x < 0$ into the downstream duct for $x > 0$. Dotted lines denote wall boundaries, solid lines denote flow in core C2 for $x < 0$ or in core C3 for $x > 0$, dashed lines denote flow in the y-direction inside the interior layer at $y = 0$, and the dot-dash line denotes flow inside the side layer at $z = -1$. In the core C3, flow at $x = 0$ is concentrated near the side at $z = -1$ and near the outer wall at $y = x+A$. As x increases, some flow enters the core from the side layer and the core flow becomes uniform over the cross-section.

in figure 3(*a*) or 3(*b*) respectively. A sketch of the flow patterns discussed here is presented in figure 4. The flow bypassing C2 through f is evident in the jumps in u at $x = 0$ in figure 3(*a*). At a particular z, the jump in u is the same at $y = A$ and at $y = 0$ (from 0 at $x = 0^-$). The jump is much larger at $z = -0.95$ than at $z = -0.05$ because the jump in $\partial p/\partial x$ is much larger near $z = -1$ than near $z = 0$. For $x < 0$, u varies linearly from 0 at $y = 0$ to the values in figure 3(*a*) at $y = x+A$; for $x > 0$, u varies linearly with y between the values presented in figures 3(*a*) and 3(*b*). The residual effect of the characteristic surfaces for $c \ll 1$ is reflected in the fact that u at $z = -0.95$ is everywhere larger than u at $z = -0.05$, except in fully developed flow. At a given x and y, the plots of u versus z are roughly parabolic with zero slope at $z = 0$ (Moon & Walker 1990). The velocity which is tangential to a wall and the distance along a wall are given by respectively multiplying the u and x in figure 3 by $\sqrt{2}$. The velocities near the outside surfaces at $z = -1$ and at $y = x+A$ are larger than those near the centreplane at $z = 0$ and near the inside surface at $y = x$, with positive implications for heat transfer in a fusion reactor cooling system. The velocities in the core C2 near $x = -A$ are very small, but this problem is easily cured by rounding the corner in the outside walls and thus eliminating much of the core C2.

The electric potentials at $z = -1$ and at the top wall at $y = x+A$ or at the bottom wall at $y = x$ are presented in figure 5. Like u, ϕ varies linearly with y. At a given x and y, ϕ varies from 0 at $z = 0$ to its maximum magnitude at $z = -1$. For fully developed flow, this variation with z is linear. For the three-dimensional disturbance,

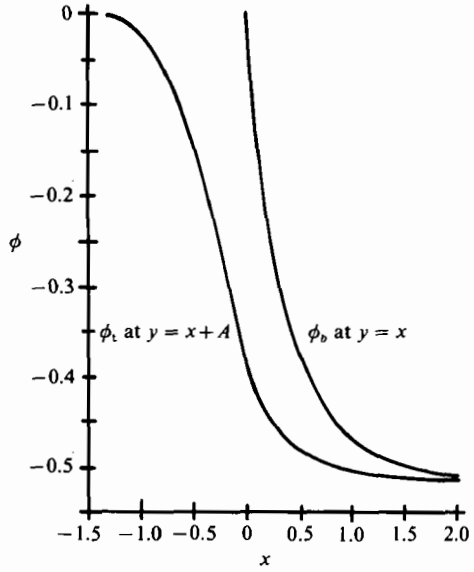

FIGURE 5. Electric potential function ϕ at $z = -1$ and at the top wall at $y = x+A$ or at the bottom wall at $y = x$.

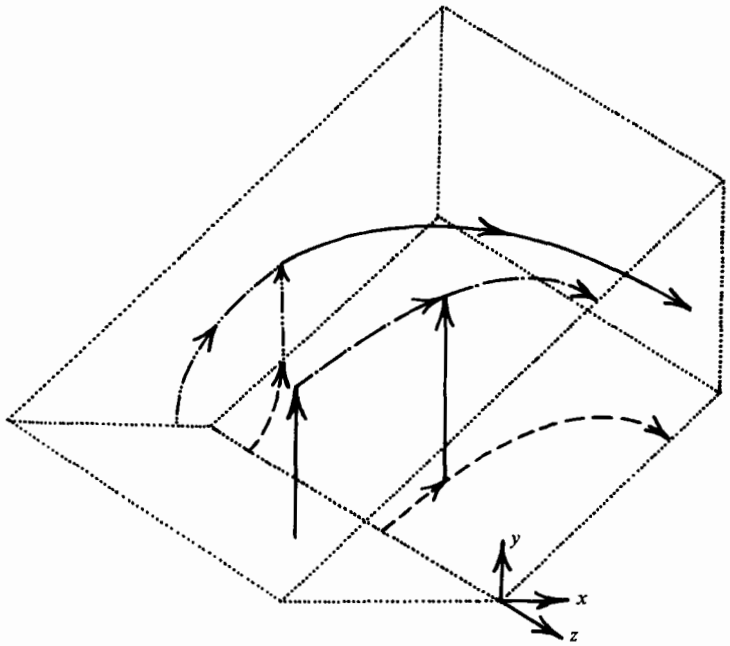

FIGURE 6. Electric current paths from the horizontal plane of symmetry $y = 0$ for $x < 0$ to the vertical plane of symmetry $z = 0$ for $x > 0$. Dotted lines denote wall boundaries, solid lines denote currents in cores C2 or C3, dashed lines denote currents inside the inner wall at $y = x$, the dot-dash line denotes current inside the outer wall at $y = x+A$, and dot-dot-dash lines denotes currents inside the sidewall at $z = -1$.

the slope $\partial\phi/\partial z$ near $z = -1$ is larger than that near $z = 0$. The electric potential is continuous across the interior layer at $x = 0$.

The electric current paths discussed here are sketched in figure 6. The three-dimensional disturbances are associated with the electric currents flowing between

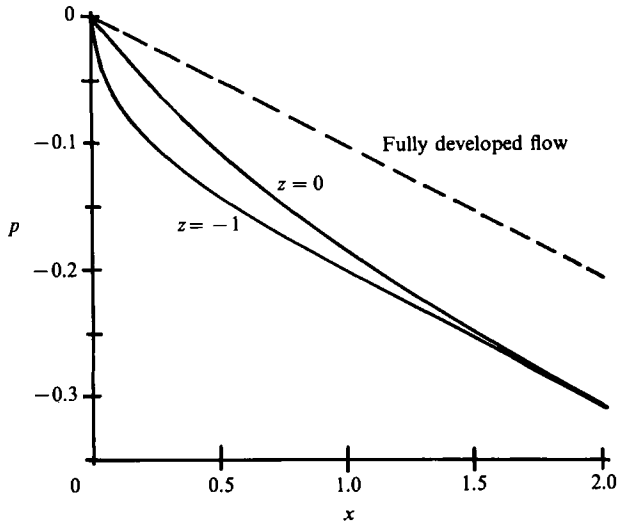

FIGURE 7. Pressure p in the core C3 at $z = 0$ and at $z = -1$. Reference pressure variation indicated by dashed line.

the far upstream flow for $y < 0$ with $\phi = -Kz$ and the far downstream flow for $y > 0$ with $\phi = Kz$. For $z < 0$, currents flow from the positive potentials upstream to the negative potentials downstream, and vice versa for $z > 0$. In the core C3 at $x = 0^+$, $p = j_x = 0$, while the electric currents in the interior and side layers are $O(M^{-\frac{1}{2}})$, so that the three-dimensional electric currents must be inside the top, bottom and side at $x = 0^+$. For $z < 0$, there are three current paths from $x = 0^+$ for $y < 0$ to $x = 0^+$ for $y > 0$. First, current can flow from the inside wall at $y = -x$ to the inside wall at $y = x$. This is clearly the path of least resistance, so that a major fraction of the three-dimensional current takes this path, which is reflected in the large value of $\partial\phi_b/\partial x$ at $x = 0^+$ in figure 5. Also the difference between ϕ_t and ϕ_b in the core C3 becomes quite large at $x = 0^+$, reflecting a large current redistribution along magnetic field lines in C1 and C3 between the higher-resistance outside-wall path and the lower-resistance inside-wall path. Second, current can flow through the outside wall at $y = -(x+A)$, along the magnetic field lines in C2 and then through the other outside wall at $y = x+A$. The magnitude of this current is reflected in the value of $\partial\phi_t/\partial x$ at $x = 0$ in figure 5, while the j_y along the C2 field lines is reflected in the values of ϕ_t for $x < 0$, divided by $(x+A)$. The third current path is through the side. Current inside the side at $x = 0$ can complete its circuit through the side itself or through the outside walls at $y = \pm(x+A)$ and along the C2 magnetic field lines. The values of p in the core C3 at $z = 0$ and at $z = -1$ are presented in figure 7. The difference, Δp, between these two lines equals the integral of j_x from $z = -1$ to $z = 0$, which is proportional to the net axial current in the core for $z < 0$ at each cross-section. As x increases, the electric circuit for the three-dimensional current is completed and $\Delta p \to 0$. The three-dimensional current in the core reaches a maximum at roughly $x = 0.2$. Since the core j_x is the same at the top and bottom for $x > 0$, it cannot represent a net current flow into or out of the top and bottom. Therefore the axial current represented by j_x in C3 must come from the side, as reflected by the large value of $j_z = -\partial p/\partial x$ at $z = -1$, for $0 < z < 0.2$. Therefore, electric currents come out of the side at $z = -1$ for $0 < x < 0.2$. This current flows in the plus x-direction inside the

core C3. Because this duct slants upward, there is an accompanying positive j_y, reflected in the difference between ϕ_t and ϕ_b in figure 5, for $x > 0$. For $x > 0.2$, the magnitude of $j_z = -\partial p/\partial x$ is larger at $z = 0$ than at $z = -1$, so that the electric current circuit for the three-dimensional current is completed across the $z = 0$ plane.

The pressure drop associated with the three-dimensional effects is the difference between the actual pressure drop and some reference pressure drop. Here the reference pressure drop is given by the pressure gradient for fully developed flow in the cores C1 and C3 and with no pressure drop in the core C2, as represented by the dashed line in figure 7. With this definition, the three-dimensional pressure drop associated with three-dimensional effects for this elbow is 0.2. Since we only consider one case, we cannot indicate how this pressure drop varies with θ, c or a.

8. Concluding remarks

If the centreline of the downstream duct is parallel to the magnetic field, corresponding to $\theta = 90°$ for either elbow in figure 1, then the pressure gradient for the downstream fully developed flow is reduced by a factor of N^{-1} to that for ordinary hydrodynamic flow. However, even a slight misalignment between the local magnetic field and the duct's centreline leads to some MHD effects, which dramatically increase the fully developed pressure gradient. Since perfect alignment cannot be achieved in practice, particularly if the direction of the magnetic field varies slightly for changing conditions, then the solutions for the forward and backward elbows for, say, $\tan\theta = 10$, represent conservative approximations to nearly parallel ducts. Nevertheless, the $\theta = 90°$ case warrants consideration as the transition between the forward and backward elbows.

Hunt & Holroyd (1977) consider a sharp elbow between two circular pipes with $\alpha = 90°$ upstream and arbitrary α downstream. Based on the small-c characteristic surfaces, they conclude that the flow becomes concentrated near $z = \pm 1$ as the downstream $\alpha \to 0$, and that the flow requires a long distance to evolve to the fully developed ordinary hydrodynamic flow. In terms of our forward elbow in figure 1 (a) for $\theta = 90°$, Holroyd (1980), citing a private communication from J. C. R. Hunt, suggests that the flow from C1 turns to flow in the y-direction inside an interior layer at $x = -a$. At $y = a$, the interior layer becomes a boundary layer adjacent to the inside wall at $x = -a$ for $y > a$. As y increases, this layer spreads gradually across the downstream duct to approach ordinary hydrodynamic flow very far downstream. Most of the fluid in $-a < x \leqslant 0$ for $O(1)\,y$ is virtually stagnant.

The arbitrary-c solution for the forward elbow for $\tan\theta = 10$ indicates that the flow in the core C2 is concentrated near the sides at $z = \pm 1$ (Moon & Walker 1990). For $c = 0.01$–0.1, this concentration involves an increase in the fraction of the total flow inside the viscous side layers and a non-uniformity in the core solution with larger u at $z = \pm 1$ than at $z = 0$. There are no high velocities inside either interior layer, and the core flow in C2 and in C3 near $x = 0$ is moderately concentrated near the outside wall, i.e. u is larger at the bottom than at the top. As θ increases past 90° and the forward elbow becomes the backward elbow with θ close to 90°, we do not expect the flow to change dramatically. The flow is still concentrated near $z = \pm 1$ in the neighbourhood of the junction. For the backward elbow for θ close to 90°, there is some vertical flow inside the interior layer at $x = 0$, but it is very small, so that virtually all the flow passes through core C2, concentrated near $z = \pm 1$, and the adjacent side layers. As θ decreases from 90° for the backward elbow, the fraction of the flow bypassing C2 and its side layers through the interior layer f increases to a

maximum at $\theta = 45°$. For $a = 1$ and $c = 0.1$, this maximum is half the flow. For all cases, the flow in cores C1 and C3 near $x = 0$ is concentrated near the outside walls. We conclude that the concentration near the sides at $z = \pm 1$ predicted by Hunt & Holroyd (1977) occurs for both the forward and backward elbows near $\theta = 90°$, and the flow concentration inside an interior layer suggested by Holroyd (1980) occurs in the backward elbow for $\theta < 90°$, with the maximum concentration for $\theta = 45°$.

For the present elbow with $c = 0.1$, the interior layer carries half the total flow. As c increases or decreases, this fraction decreases or increases, respectively. For much smaller values of c or for insulating walls with $M = 10^4$–10^5, the interior layer carries virtually all the flow from C1 to C3, and the fluid in the triangular protuberance for $x < 0$ is virtually stagnant, i.e. the predictions of the small-c solutions with the characteristic surfaces are realized. If insulating coatings are developed for fusion-reactor cooling systems, the pressure drops will be greatly reduced, but the danger of stagnant pockets will be increased.

Combining the present results and the forward-elbow results (Moon & Walker 1990), we can answer the three questions of importance for the fusion reactor designs. The three-dimensional pressure drops associated with these elbows are relatively modest, corresponding to the fully developed pressure drop for the nearly perpendicular duct over one or two characteristic lengths at most. The flows in core C3 and the adjacent side layers only deviate from fully developed for $0 < x < 2$. The flow is generally more concentrated near the outside than near the inside walls and near $z = \pm 1$ than near $z = 0$, with positive implications for heat transfer. For the backward elbow for $\theta = 45°$ there is very little flow in C2 near $x = -A$, but this hot spot is easily eliminated by rounding the outside corner.

This research was supported by the Fusion Power Program at Argonne National Laboratory. Dr B. F. Picologlou of Argonne National Laboratory provided valuable assistance with the rationale and formulation of this problem.

REFERENCES

HOLROYD, R. J. 1980 An experimental study of the effects of wall conductivity, non-uniform magnetic fields and variable area ducts on liquid metal flows at high Hartmann numbers. Part 2. Ducts with conducting walls. *J. Fluid Mech.* **96**, 355.

HOLROYD, R. J. & WALKER, J. S. 1978 A theoretical study of the effects of wall conductivity, non-uniform magnetic field and variable-area ducts on liquid-metal flows at high Hartmann number. *J. Fluid Mech.* **84**, 471.

HUA, T. Q. & PICOLOGLOU, B. F. 1990 MHD flow in a manifold and multiple rectangular coolant ducts of self-cooled blankets. *Fusion Technol.*

HUA, T. Q., WALKER, J. S., PICOLOGLOU, B. F. & REED, C. B. 1988 Three-dimensional magnetohydrodynamic flows in rectangular ducts of liquid-metal-cooled blankets. *Fusion Technol.* **14**, 1389.

HUNT, J. C. R. & HOLROYD, R. J. 1977 Applications of laboratory and theoretical MHD duct flow studies in fusion reactor technology. *Culham Laboratory Rep.* CLM-R169.

KULIKOVSKII, A. G. 1968 Steady, slow flows of conducting fluid at large Hartmann number. *Mekh. Zhid. i Gaza* **2**, 3.

MALANG, S. *et al.* 1988 Self cooled liquid-metal blanket concept. *Fusion Technol.* **14**, 1343.

MOON, T. J. & WALKER, J. S. 1990 Liquid metal flow through a sharp elbow in the plane of a strong magnetic field. *J. Fluid Mech.* **213**, 397.

PICOLOGLOU, B. F., REED, C. B., DAUZVARDIS, P. V. & WALKER, J. S. 1986 Experimental and analytical investigation of magnetohydrodynamic flow near the entrance of a strong magnetic field. *Fusion Technol.* **10**, 860.

SHERCLIFF, J. A. 1956 The flow of conducting fluids in circular pipes under transverse magnetic fields. *J. Fluid Mech.* **1**, 644.

SMITH, D. L. *et al.* 1985 Blanket comparison and selection study. *Fusion Technol.* **8**, 1.

TALMAGE, G. & WALKER, J. S. 1988 Three-dimensional laminar MHD flow in ducts with thin metal walls and strong magnetic fields. Liquid metal flows: magnetohydrodynamics and applications. *Prog. Astro. Aero* **111**, 3.

TALMAGE, G., WALKER, J. S., BROWN, S. H. & SONDERGAARD, N. A. 1989 Liquid metal flows in current collectors for homopolar machines: fully developed solutions for the primary azimuthal velocity. *Phys. Fluids* A **1**, 1268.

WALKER, J. S. 1981 Magnetohydrodynamic flows in rectangular ducts with thin conducting walls: Constant-area and variable-area ducts with strong uniform magnetic field. *J. Méc.* **20**, 79.

WALKER, J. S. & LUDFORD, G. S. S. 1975 MHD flow in circular expansions with thin conducting walls. *Intl J. Engng Sci.* **13**, 261.

WALKER, J. S., LUDFORD, G. S. S. & HUNT, J. C. R. 1971 Three-dimensional MHD duct flows with strong transverse magnetic fields. Part 2. Variable-area rectangular ducts with conducting sides. *J. Fluid Mech.* **46**, 657.